Publishing House
AKAPIT

COMPUTER METHODS IN MATERIALS SCIENCE

Informatyka w Technologii Materiałów

Vol. 10, 2010, No. 1

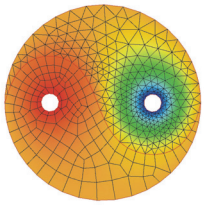

EXPERIMENTAL VERIFICATION RESULTS OF REAL AND EQUIVALENT DRAWBEADS NUMERICAL SIMULATIONS

ZBIGNIEW ZIMNIAK*, DAWID RUTKOWSKI

Institute of Production Engineering and Automation, Wroclaw University of Technology
ul. Łukasiewicza 5, 50-371 Wroclaw, Poland
**Corresponding Author: zbigniew.zimniak@pwr.wroc.pl*

Abstract

In sheet metal forming, drawbeads play an important role in material flow control. In this paper the results of simulations of drawbeads and equivalent drawbeads are experimentally verified. Strain and thickness variations were measured for a rectangular drawpiece. FEM modelling was done with commercial software LS-DYNA using explicit and implicit FEA codes. Three-dimensional numerical simulations were run using Hill's 1948 anisotropic yield function and the Barlat-Lian (1989) constitutive model. Calculations relating to the gravitational force loading and the drawing process were done using the explicit method and the spring back simulation was carried out using the implicit method. The numerical simulation results were verified through the measurement of principal strains in selected cross sections of the drawpiece. As regards the principal strain distributions and the final drawpiece dimensions, good agreement between the experimental measurements and the FEM calculations was obtained. The best agreement for real drawbeads results occurred under the Barlat-Lian criterion. In the model an equivalent drawbead is represented by a line on the surface of the tools, along which the prescribed drawbead restraint force (DBRF) were exerted. This means that calculating the drawbead restrain force from formula and describing the sheet material by means of the Barlat-Lian criterion one can successfully use equivalent drawbeads.

Key words: deep drawing, drawbead, equivalent drawbead, finite element method

1. INTRODUCTION

Drawbeads play a key role in the forming of metal sheets for car body components. In order to select a proper drawbead shape and location many expensive tool prototypes need to be made. In order to avoid this and to correctly design the forming process, FEM simulations are carried out (Zimniak, 2006). In numerical simulations drawbeads can be faithfully reproduced geometrically, but in order to reduce the computing time the so-called equivalent beads are used (Chen & Liu, 1997; Firat, 2008; Sun et al., 2010).

The function of a drawbead located on the blankholder's surface is to control the material flow into the die. The drawbead introduces additional forces (acting in the direction opposite to that of forming) tensioning the metal sheet, and a series of local processes: sheet bending, levelling and bending in the opposite direction. As the metal sheet passes over the drawbead it becomes thinner and is additionally strain hardened. Drawbeads function as brakes and generate additional tensile stresses, whereby they prevent folds from forming on the drawpieces. Folding during forming is the result of different resistances to material flow in the different parts of the drawpiece. In order to ensure a possibly uniform distribution of flow resistance, drawbeads are used in the places where the material flows more easily. For this purpose the geometric location of

ISSN 1641-8581

drawbeads is optimized by means of various numerical algorithms (Liu et al., 2002; Marczewski & Sosnowski, 2003; Sheriff et al., 2008). Also drawpiece spring back can be minimized through the optimum design of the drawbeads (Song et al., 2005).

As part of this research the results of the FEM modelling of drawbeads (including equivalent drawbeads) by means of the LS-Dyna software were experimentally verified. Also the numerical calculation results for metal sheet formability, geometric dimensions and principal strains were experimentally verified.

2. NUMERICAL MODEL OF FORMING PROCESS WITH DRAWBEADS

A rectangular drawpiece with four drawbeads was used in the FEM analysis of the forming process. Geometrical dimensions of drawpiece were 200x150x50 mm. The calculation model components, the adopted arrangement of the drawbeads and their basic geometric dimensions are shown in figure 1.

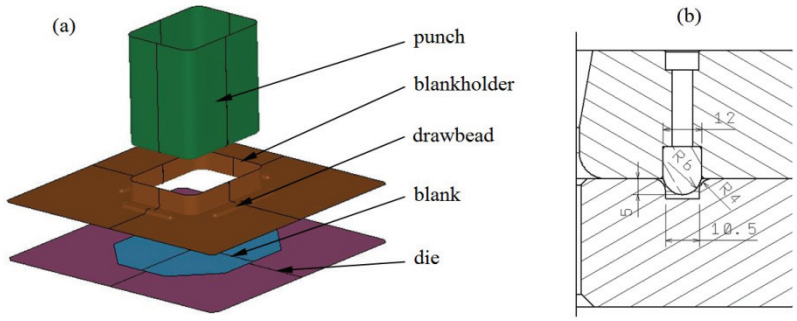

Fig. 1. *Tooling system a), and geometry of drawbeads b)*

Sheet metal forming was simulated using the LS-Dyna software and two computing methods: the explicit dynamic analysis and the implicit static analysis. The finite element mesh was automatically refined in the course of computing. The tools: the punch, the die and the blankholder were assumed rigid. The deformable element was the metal sheet. One fourth of the solution space was analyzed under appropriate model symmetry conditions. Shell finite elements with four integration points (LS-Dyna elements type 16) on the plane and ten integration points along the thickness of the shell (to better render the variation in stress along sheet thickness during spring back) were used (LS-DYNA, 2006). Element type 16 is a fully integrated shell with assumed strain interpolants used to alleviate locking and enhance in-plane bending behavior. It uses a local element coordinate system (similar to the used for the Belytschko-Tsay element) that rotates with the material to account for rigid body motion and automatically satisfies frame invariance of the constitutive relations. Two models describing the plasticity surface of the material were adopted. One of the models was Hill's (1948) anisotropic function (LS-Dyna MAT37):

$$F(\sigma_{22}-\sigma_{33})^2 + G(\sigma_{33}-\sigma_{11})^2 + H(\sigma_{11}-\sigma_{22})^2 + 2L\sigma_{23}^2 + 2M\sigma_{31}^2 + 2N\sigma_{12}^2 - 1 = 0 \quad (1)$$

where: the constants F, G, H, L, M, and N are related to the yield stress. The other model was the Barlat-Lian (1989) constitutive model (LS-Dyna MAT36):

$$a|K_1 + K_2|^m + b|K_1 - K_2|^m + c|2K_2|^m = 2\sigma_p^m \quad (2)$$

where:

$$K_1 = \frac{\sigma_{11} + h\sigma_{22}}{2};$$

$$K_2 = \sqrt{\left(\frac{\sigma_{11} - h\sigma_{22}}{2}\right)^2 + p^2\tau_{12}^2} \quad (3)$$

a, b, c, h – constants defined by plastic strain ratios: r_0, r_{45} and r_{90}, m – a constant, σ_p – yield stress.

One millimetre thick steel DC04 (EN10130) was adopted as the sheet material. A constant Coulomb friction coefficient of 0.125 was assumed. The blankholder force was 64000 N. The basic material specifications used in the simulations are shown in table 1.

Table 1. *Material data*

Young's modulus (GPa)	207.3
Poisson's ratio	0.28
Mass density (kg/m^3)	7850
r-Value	r_0= 2.582 , r_{45}= 1.921, r_{90}= 2.193, r= 2.154
Strength coefficient and strain hardening exponent	K= 542.3 MPa, n= 0.19

The work-hardening curve was entered as an experimental data table into the FEM programme. In total there were 64713 finite elements, and 71979 elements after remeshing process. Calculations relat-

ing to the gravitational force loading and the drawing process were done using the explicit method and the springback simulation was carried out using the implicit method. The obtained effect of the blank deformation under the gravitational loading was negligible.

3. FEM CALCULATION RESULTS

The results from the simulation of rectangular drawpiece forming with real geometry drawbeads after springback are shown below (figure 2). The areas of different formability for the two material models are represented by shades of grey. A larger area of formability occurred in the case of the Barlat-Lian criterion.

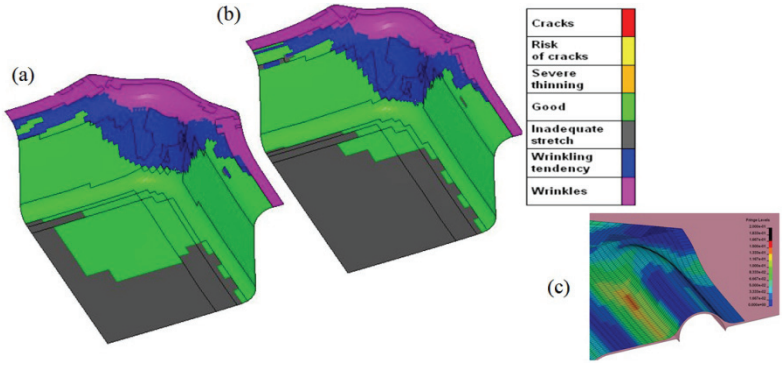

Fig. 2. FLD formability results: Barlat-Lian criterion a), Hill criterion b). Magnified zone of the drawbead showing effective strain distribution c)

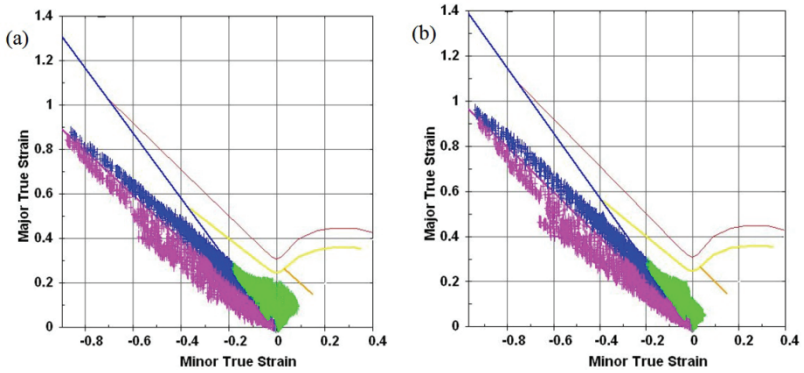

Fig. 3. Forming limit diagrams for: Barlat-Lian criterion a), Hill criterion b)

Figure 3 shows forming limit diagrams for the material models with marked principal strain values determined by the simulations. As one can see, closest to the FLD are the calculation points approaching the plane state of strain, determined for the Barlat-Lian criterion.

Figure 4 shows the percentage thinning of the sheet in the considered cases. It appears from the FLD that the largest thinning occurs for the Barlat-Lian criterion.

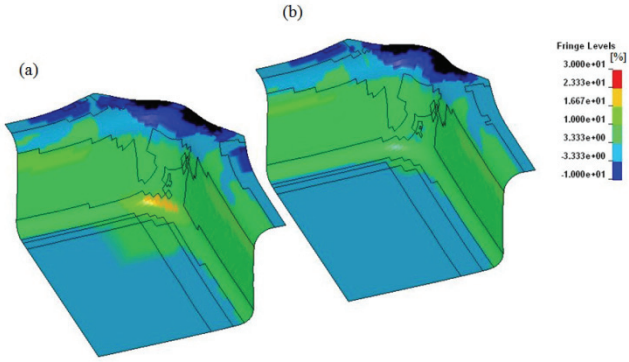

Fig. 4. Thickness distribution for: Barlat-Lian criterion a), Hill criterion b)

The above results show that under the Barlat-Lian criterion the distance to the FLD is the shortest, but there is still no risk of drawpiece fracture. Experimental verification is needed to check the simulation results.

4. EXPERIMENTAL VERIFICATION OF NUMERICAL SIMULATION RESULTS

The numerical simulation results (at the external surface of shell elements, according with the experiment) were verified through the measurement of principal strains in selected cross sections of the drawpiece. Figure 5 shows the lines along which measurements were made. Strains and geometry were measured using respectively the coordination lattice method and a measuring machine.

The results for the measurement line running along the drawpiece are shown in figure 6 (the Barlat-Lian criterion) and in figure 7 (the Hill criterion). It appears from the comparison that there is better agreement between the experimental results and the theoretical results under the Barlat-Lian criterion. This applies to the two principal strain components: ε_1 and ε_2. Experimental measurements of strains were performed by excluding the range of distance 120-140 mm. The curve approximation of experimental strains is shown only as pictorial.

Qualitatively similar results were obtained for the other measurement lines. The agreement for the two strain components can be considered as good.

The numerical simulation results were also verified by comparing the calculated drawpiece geomet-

ric dimensions after spring back with the measured ones. As an illustration, such a comparison for the longitudinal measurement line is shown in figure 8. Very good agreement between the experimental and simulation results was obtained under the Barlat-Lian criterion. This was also found for the other measurement lines.

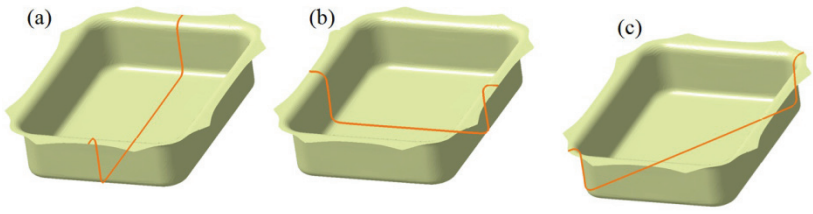

Fig. 5. Location of measurement line: longitudinal a), transverse b), skew c)

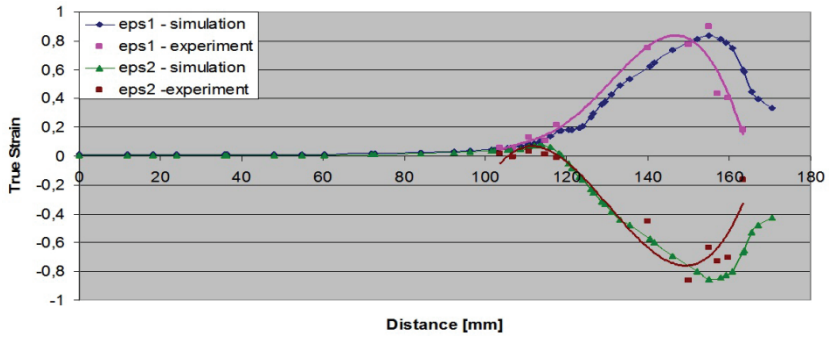

Fig. 6. Deformation diagrams for Barlat-Lian criterion – longitudinal measurement line

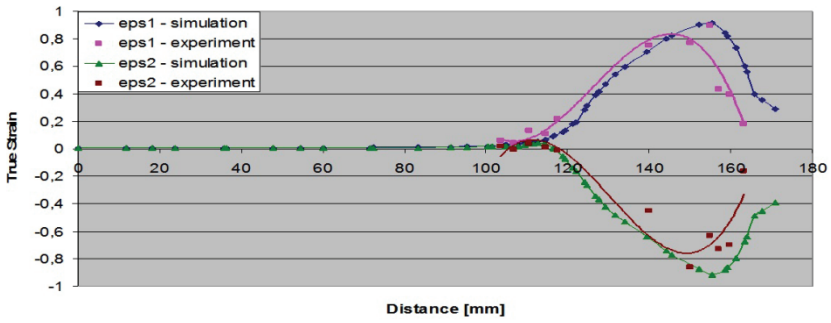

Fig. 7. Deformation diagrams for Hill criterion – longitudinal measurement line

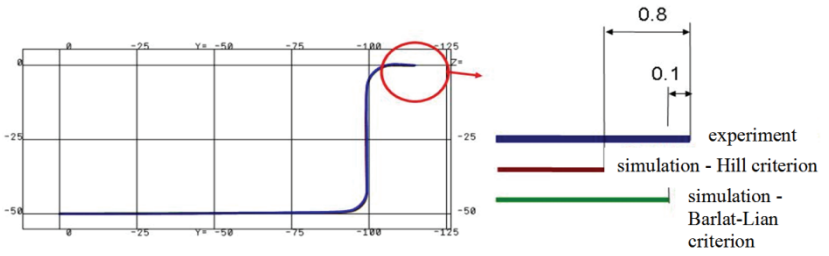

Fig. 8. Comparison of theoretical results with experimental results for longitudinal drawpiece cross section

5. SIMULATION OF FORMING PROCESS WITH EQUIVALENT DRAWBEADS

Thanks to the use of an equivalent drawbead larger finite elements can be used for the simulation of the drawing of the drawpiece over the drawbead whereby the computing time is greatly reduced. This is particularly important when complicated drawpiece shapes (very large computing problems) are to be analyzed.

In the model an equivalent drawbead is represented by a line on the surface of the tools, along which the prescribed drawbead restraint force (DBRF) will be exerted. The force is distributed among the particular finite element nodes which at a given instant intersect the equivalent drawbead line.

The implementation of drawbeads (LS-Dyna software) is based on elastic-plastic interface springs and nodes-to-surface contact. The area of the blank under the drawbead is taken as the master surface. The drawbead is defined by a consecutive list of nodes that lie along the drawbead. The drawbead line is discretized into points that become the slave nodes to the master surface. The dense distribution of point leads to a smooth drawbead force distribution which helps avoid exciting the zero energy (hourglass) modes within the shell elements in the workpiece.

DBRF is usually a function of the properties of the sheet material, the shape of the drawbead and the friction conditions. A DBRF value of 140 N/mm, determined from the formula (Weidemann, 1978; Shuhui et al., 2002):

$$DBRF = tw\left\{\frac{2\mu P}{t}e^{4\mu\varphi} + \frac{2\sigma_p}{\sqrt{3}}\left[\left(\left(\frac{e^{\mu\varphi}}{4\left(R_g+\frac{1}{2}t\right)} + \frac{1}{4\left(R_g+\frac{1}{2}t\right)} + \right.\right.\right.\right.$$

$$\left.\left.\left.\left.\frac{1}{4\left(R_b+\frac{1}{2}t\right)}\right)e^{2\mu\varphi} + \frac{1}{4\left(R_g+\frac{1}{2}t\right)} + \frac{1}{4\left(R_g+\frac{1}{2}t\right)}\right)e^{\mu\varphi} + \frac{1}{4\left(R_g+\frac{1}{2}t\right)}\right]\right\} \quad (4)$$

was used in the simulation. In the above formula: t – is sheet thickness, w – drawbead length, μ – a friction coefficient, φ – bending angle of the blank and P – an equivalent blankholder force per unit length (the binder holding force is applied to the flat surface of the blank). The other parameters in formula (4) represent the drawbead's geometric dimensions (Weidemann, 1978). The value of blankholder force per unit length in formula (4) was assumed the same as in case of numerical calculation with real drawbead.

The formability results for the real and equivalent drawbead under the Barlat-Lian criterion are compared in figure 9. The equivalent drawbeads located exactly in the places previously occupied by the real drawbeads are shown in figure 9b. The formability areas show slight differences between the two cases. Also the geometric dimensions show slight differences between the two cases (figure 10). The drawpiece flange width (the drawbead) is slightly longer for the equivalent drawbead simulation results.

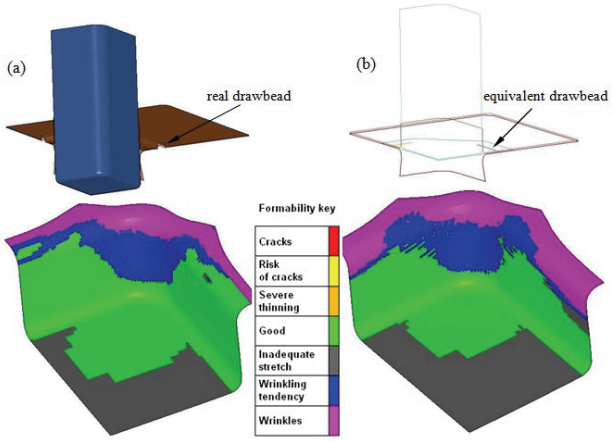

Fig. 9. *Comparison of formability results for drawpieces with real a) and equivalent drawbead b)*

Comparing the times of numerical calculations, for 3D drawbead it was 52 min. 48 sec., and for equivalent drawbead 27 min. 21 sec. It shows a significant reduction in the time of numerical calculations.

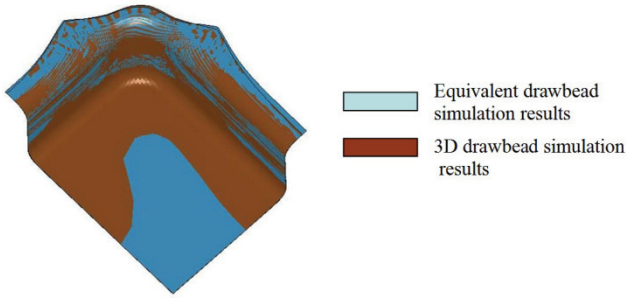

Fig. 10. *Comparison of results for real and equivalent drawbead*

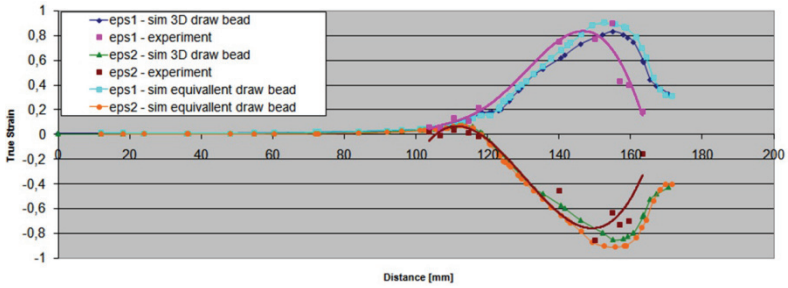

Fig. 11. *Deformation diagrams for Barlat-Lian criterion – comparison of results for 3D, experimental and equivalent drawbeads*

A very good indication of the correctness of equivalent drawbead model is comparison results of main strains with results for real drawbead and experimental results (figure 11).

The use of equivalent drawbeads did not lead to any large differences in the results in comparison with the ones obtained using the real drawbeads. This means that through the smart use of equivalent drawbeads one can obtain correct forming process simulation results, which has been experimentally verified.

6. CONCLUSION

The correctness of the FEM modelling of real and equivalent drawbeads has been experimentally verified. As regards the principal strain distributions and the final drawpiece dimensions, good agreement between the experimental measurements and the FEM calculations was obtained. The best agreement for these results occurred under the Barlat-Lian criterion. The latter criterion was used to compare the forming process calculation results for real and equivalent drawbeads. The calculation results are very similar for the two cases. This means that calculating the drawbead restrain force from formula

(4) and describing the sheet material by means of the Barlat-Lian criterion one can successfully use equivalent drawbeads. It is necessary to use the latter when a forming technology is to be developed for very complicated drawpiece shapes since through the use of equivalent drawbeads the computing time can be greatly reduced.

REFERENCES

Barlat, F., Lian, J., 1989, Plastic behavior and stretchability of sheet metals, a yield function for orthotropic sheet under plane stress condition, *Int. J. Plasticity*, 5, 51-63.

Chen, F., Liu, J., 1997, Analysis of an equivalent drawbead model for finite element simulation of a stamping process, *Int. J. Mach. Tools Manufact.*, 37(4), 409-423.

Firat, M., 2008, An analysis of sheet drawing characteristics with drawbead elements, *Computational Mater. Science*, 41, 266-274.

Hill, R., 1948, *A theory of the yielding and plastic flow of anisotropic metals,* Proc. Roy. Soc. London.

Liu, G., Lin, Z., Bao, Y., 2002, Optimization design of drawbead in drawing tools of autobody cover panel, *J. Eng. Mater. Technol.*, 124, 278-285.

LS-DYNA, 2006, Theory Manual, Compiled by Hallquist O.J., Livermore Software Technology Corporation.

Marczewski, A., Sosnowski, W., 2003, Analiza wrażliwości w zastosowaniu do optymalizacji położenia progów ciągowych, *Materiały Konferencji FiMM, nt. Fizyczne i Matematyczne Modelowanie Procesów Obróbki Plastycznej*, Oficyna Wydaw. PWarsz., Warszawa, 163-168 (in Polish).

Sheriff, N.M., Ismail, M.M., 2008, Numerical design optimisation of drawbead position and experimental validation of cup drawing process, *J. Mater. Process. Technol.*, 206, 83-91.

Shuhui, L., Zhongqin, L., Weili, X., Youxia, B., 2002, An improved equivalent drawbead model and its application, *J. Mater. Process. Technol.*, 121, 308-312.

Song, J.H., Huh, H., Kim, S.H., Park, S.H., 2005, Springback reduction in stamping of front side member with a response surface model, *Proc. Conf. NUMISHEET*, eds, Smith, L.M., Smith Lorenzo, M., Zhang, L., Detroit, 303-308.

Sun, G., Li, G., Gong, Z., Cui, X., Yang, X., Li, Q., 2010, Multiobjective robust optimization method for drawbead design in sheet metal forming, *Materials and Design*, 31, 1917-1929.

Weidemann, C., 1978, The blank holder action of drawbeads, *Proc. of the 10th Biennial IDDRG Congress,* eds, Charles van Riper III, Colorado Plateau, 79-85.

Zimniak, Z., 2006, Computer aided sheet metal forming process design, *Computer Methods in Materials Science*, 6(1), 33-41.

EKSPERYMENTALNA WERYFIKACJA WYNIKÓW NUMERYCZNEJ SYMULACJI RZECZYWISTYCH I ZASTĘPCZYCH PROGÓW CIĄGOWYCH

Streszczenie

Progi ciągowe odgrywają bardzo ważną rolę w kontrolowaniu płynięcia materiału podczas procesów głębokiego tłoczenia blach. W pracy przedstawiono eksperymentalną weryfikację wyników numerycznej symulacji progów ciągowych oraz zastosowanych zastępczych progów ciągowych. Dla analizowanej wytłoczki prostokątnej dokonano pomiarów rozkładów odkształceń głównych oraz zmian grubości blachy. Modelowanie MES zostało przeprowadzone z użyciem komercyjnego programu LS-DYNA, wykorzystującego do obliczeń numerycznych kody typu explicit i implicit. Trójwymiarowe numeryczne symulacje przeprowadzono używając warunków plastyczności podanych przez Hilla w roku 1948 oraz przez Barlata i Liana z roku 1989. Obliczenia dotyczące obciążenia siłą grawitacji oraz procesu samego ciągnięcia wykonano z zastosowaniem metody explicit, a symulację sprężynowania powrotnego przeprowadzono metodą implicit. Weryfikację doświadczalną wyników obliczeniowych przeprowadzono poprzez pomiar odkształceń głównych w wybranych przekrojach wytłoczki. Na podstawie otrzymanych wyników badań dla progów rzeczywistych, dotyczących rozkładów odkształceń głównych oraz końcowych wymiarów geometrycznych wytłoczek, można stwierdzić dobrą zgodność wyników pomiarów doświadczalnych z obliczeniami MES. Najlepszą zgodność tych wyników uzyskano dla kryterium Barlata-Liana. Zastępczy próg ciągowy był określany w modelu przez linię leżącą na powierzchni narzędzi, wzdłuż której wywierana była zadana wartość siły oporu progu ciągowego (drawbead restraint force – DBRF). Można więc z powodzeniem stosować zastępcze progi ciągowe z zastosowaniem przyjętego w pracy wzoru na siłę oporu progu oraz z opisem materiału blachy za pomocą kryterium Barlata-Liana.

Received: February 28, 2010
Received in a revised form: June 23, 2010
Accepted: June 28, 2010